Desalination and Water Treatment
www.deswater.com

doi: 10.1080/19443994.2015.1130656

57 (2016) 22321–22328
October

Taylor & Francis
Taylor & Francis Group

Simulation of adsorption of antimony on zero-valent iron nanoparticles coated on the industrial minerals (kaolinite, bentonite and perlite) in mineral effluent

Setareh Saeidnia[a], Gholamreza Asadollahfardi[a,*], Ahmad Khodadadi Darban[b]

[a]*Department of Civil Engineering, Kharazmi University, Karaj, Iran, Tel. +98 9358139293; email: setare.saeidnia@yahoo.com (S. Saeidnia), Tel. +98 9121192424; email: asadollahfardi@yahoo.com (G. Asadollahfardi)*
[b]*Department of Mining Engineering, Tarbiat Modares University, Tehran, Iran, Tel. +98 9123908067; email: akdarban@modares.ac.ir*

Received 25 May 2015; Accepted 4 December 2015

ABSTRACT

Antimony is one of the most toxic pollutants existing in the industrial and mineral effluents threatening human and other creatures' life. Removal of antimony has been performed using various methods. One of the methods of removing antimony from mineral effluent is surface adsorption. We simulated the absorption of antimony in the presence of nano-zero-valent iron (nZVI) coated with industrial minerals such as kaolinite, bentonite, and perlite from mineral effluent using VISUAL MINTEQ 3.1 software. Our aim was to determine the factors affecting the absorption of antimony from mineral effluent by applying simulation. The simulation was performed using an adsorption of diffuse layer model. The results of simulation indicated that the nZVI concentration and pH factor are effective in the absorption of antimony. The simulation presented by increasing the pH from 1 to 2 and by rising the concentrations of nZVI from 7.5 to 12.5 mg/l causes the rate of antimony absorption to increase. The absorption capacity for nZVI coated with kaolinite, bentonite, and perlite were 3.92, 2.46, and 3.1 milligrams per gram of absorbent and the greatest amount of antimony removal was associated with perlite composite. In all cases, the coefficient of determination (R^2) between laboratory results and model predictions was more than 0.9.

Keywords: Antimony; Mineral effluent; Nano-zero-valent iron; Adsorption; VISUAL MINTEQ

1. Introduction

Almost all gold plants have effluent containing antimony that enters into the environment and is considered as one of the toxic elements. The waste of these plants is extremely toxic and may contain risks of environmental pollution if antimony is dissolved [1]. Antimony is a metalloid that is harmful to human and plant health. Breathing antimony in composition with oxygen in the gas phase is considered to be a public health risk [2]. Therefore, assessment of the environmental impact and reduction or elimination of antimony from mineral water using an appropriate method are necessary [3]. Antimony compounds are often classified according to their oxidation state: Sb (III) and Sb(V). The +5 oxidation state is more stable. This metalloid is sensitive to oxidation–reduction reactions. Being spread, mobility and species depend on

*Corresponding author.

various factors such as the pH of the environment, the presence of other ionic species, and the chemistry of the solution. Antimony is rarely observed in nature as a pure element and antimony(III) and antimony(V) are readily hydrolyzed in aqueous solutions [4].

Water Resources Research Center, United States of America, has reported that the capacity of antimony existing in food and water that can be tolerated by the human body is 0.1 mg and for antimony in the air is 0.0017 mg [5]. Several methods are available to remove antimony from water and wastewater. Among them, the absorption methods have attracted the attention of many fans in recent years because of simple, low-cost, and effective methods for removing heavy metal ions and organic compounds at low and average concentrations [6]. Factors affecting adsorption include the type and characteristics of the absorbent and absorbed, the degree of mixing in the liquid phase, the pH, and the temperature [7].

Nanotechnology is considered a priority and strategic technology for all countries due to the diverse application areas and direct impact on most industries and sciences. Nanomaterials have very extensive surfaces compared to material in large dimensions [8]. Zero-valent iron nanoparticles are capable of decomposing organic pollutants and absorbing inorganic pollutants. Some of these nanoparticles may be covered by different surface modifiers to control their reactions and mobility [9]. Modified iron nanoparticles have been produced to speed up clean-up and restoration. Kaolinite, bentonite, and expanded perlite industrial minerals are clay minerals in the soil, which play an important role in controlling pollutants through geochemical processes, especially the absorption [10]. These minerals have the ability to act as an absorbent and easy access through structural stability and geochemical conditions. Due to these properties, clay can be used to host nano-zero-valent iron (nZVI) in clearing systems [11].

Ilavsky [12] reviewed antimony removal from water in Slovakia using Bayoxide E33 absorbents (granulated medium based on ferric oxides) and Granular Eisen Hydroxyde (GEH). The results indicated that at the pH (range 6.8–6.9 during the test), Bayoxide absorption capacity was 27.78 micrograms per gram and the absorption capacity of GEH was 85.04 micrograms per gram, respectively [12]. Anjam and Datta [13] studied the trivalent antimony adsorption kinetics on montmorillonite for reaction time of 10–180 min. They concluded that about 99% of synthesis solution antimony, 100 mg per liter, is removed using the adsorbent [13]. Leng et al. [14] were successful in removing the trivalent antimony using graphene. Their experimental data described that adsorption of antimony on graphene obeys a pseudo-second-order kinetic model [14]. Salam and Mohamed removed trivalent antimony using multi-walled carbon nanotubes [15]. Sari et al. [16] used expanded perlite as a trivalent antimony; they obtained the optimal capacity of 54.4 milligrams per gram of adsorbent [16]. Xi et al. [17] removed pentavalent antimony using kaolinite. They obtained an optimal pH of 3.6 for the removal so that 75% of antimony was removed at this pH [17]. Vithanage et al. [18] investigated surface complexation modeling and spectroscopic evidence of antimony adsorption on iron-oxide-rich red earth soils. Successful data modeling using the 2-pK diffuse layer model (DLM) with the FITEQL revealed that absorption occurs through the formation of bidentate mononuclear and binuclear complexes. Also, the model simulation indicated a high absorption affinity of antimony to the FeOH sites and the highest absorption of Sb(V) at acidic pH of about 4 to 6 [18]. Safavi [19] conducted a simulation of a cyanide adsorption process on titanium dioxide nanoparticles using VISUAL MINTEQ software. Also, the coefficient of determination (R^2) between her results of simulation and experiments was equal to 0.9 which indicates that her model was acceptable. The results obtained from the use of 2-pK CCM and 2-pK DLM surface complexes presented the same results and two linear and Freundlich adsorption models predicted results that matched the experimental results [19]. Antimony is more serious in Azerbaijan province in Iran owing to the existence of a large number of antimony mines. However, despite the evident potential Sb(V), its adsorption simulation from Zarshouran Gold Mineral Processing Wastewater Plant by (nZVI) coated on industrial mineral has not been reported to date.

The simulation of antimony absorption using MINTEQ software has never been carried out previously. The first objective of this study was to simulate the absorption of antimony in the presence of nZVI which was coated on kaolinite, bentonite, and perlite from mineral wastewater using the VISUAL MINTEQ 3.1 software [20]. This software was used to study the chemical equilibrium problems. The second aim was to determine factors affecting the adsorption rate using a DLM.

2. Methods

MINTEQ is a geochemical software based on chemical equilibrium developed by American Environmental Agency. Types of absorption patterns, mass balance between solid or liquid and gas phases, and equations for mass interplay are available from the software. In addition, the software contains algorithms

to check and correct the equilibrium constants. In this model, no time is available and the circumstances are not kinetic and the maximum absorption that took place at the time of equilibrium was assumed [20].

Because of the high possibility of interactions between the ions and inorganic and organic solids in natural systems, the models are used as a tool to quantify and predict the behavior of ions in solution and their interactions with other particles. For this reason, in recent decades, several models have been proposed for the analysis of chemical reactions. The DLM is one of the various models that are available to explain ion absorption data [21].

The DLM was first proposed by Stumm et al. [22] and then revised by Dzomback and Morel [23]. In this model, all the ions are located on the surface and just from within the core complex. The double-layer model usually considers two adsorption sites with low absorption affinity and high adsorption affinity [23]. The ionic strength of this model affects the model through parameter I in the layer d. Thus, this model can be used under varying conditions of low ionic strength. Eq. (1) indicates the relationship between the load in the layer (d) and ionic strength (I) (M):

$$\sigma_d = -0.1174 \times \sqrt{I} \times \sinh\left(\frac{Z \times F \times \Psi_d}{2 \times R \times T}\right) \ (\mathrm{C/m^2}) \tag{1}$$

where σ_d is the diffusion layer load (C/m^2), Z is the electrolyte capacity assumed to be single, and I is the ionic strength (M). F is the Faraday constant (J/volt equiv), R is the gas constant (J/K mol), T is the absolute temperature (K), and Ψ_d (volt) is the electrostatic potential of layer d.

Ψ_d is the potential at the surface of the absorbent.

The assumptions are as follows [24]:

(1) The surface sites are amphoteric (a site can be positive, neutral, or negative).
(2) Surface complexes are monodentate within the sphere (only one atom is connected to the central metal atom).
(3) Two electrostatic plates are available in this model:
(a) The surface electrostatic page adsorbs H, OH, and other ions.
(b) The d electrostatic surface adsorbs ions with an opposite charge.
(4) The relationship between the charge and the electrostatic potential in the diffuse layer is explained by the Gouy–Chapman theory. Gouy [25] and Chapman [26] presented the effect of surface charge on ion adsorption using an electric double layer theory, which was then reviewed by Stern [20].
(5) The base state of the model is the zero load for the surface forms and a very dilute solution, for the solution forms.

The MINTEQ software contains various absorption models, an organic material, a powerful database achieved acceptable agreement with the experimental data [20]. In this simulation, we used the experimental data which were conducted by Nosrati [24] and Nosrati et al. [27]. Creating chemical equilibrium (reversible reaction), failure in considering the time (there are no synthetic reactions), 0–99˚C temperature restriction, and limited ionic strength are some of the limitations of this software.

2.1. Model efficiency

We used a coefficient of determination, R^2, index of agreement (IA) for the efficiency of the models [28–30]:

$$R^2 = \left(\frac{\sum_{i=1}^{i}(A_t - \bar{A})(F_t - \bar{F})}{(\sum_{i=1}^{n}(A_t - \bar{A})^2)\sum_{i=1}^{i}((F_t - \bar{F})^2)^{0.5}}\right)^2 \tag{2}$$

$$IA = 1.0 - \frac{\sum_{t=1}^{N}(A_t - F_t)^2}{\sum_{t=1}^{N}(|F_t - \bar{A}) + |A_t - \bar{A})|^2} \tag{3}$$

where A_t, F_t, and $\bar{A}$ are observed data, predicted data, and mean observed data, respectively.

We also applied Eq. (5) for efficiency of the models.

$$P = \frac{100}{N}\sum \frac{|C_{t,\mathrm{expt.}} - C_{t,\mathrm{pred.}}|}{C_{t,\mathrm{expt.}}} \tag{4}$$

where $C_{t,\mathrm{expt.}}$ is the experimental concentration at any time, $C_{t,\mathrm{pred.}}$ is the corresponding predicted concentration according to the equation under study with best fitted parameters, and N is the number of observations, and the fit accepted to be good when P is below 5.

2.2. Applied experimental data for simulation [24,27]

We used the data from Nosrati [24] experiments and Nostrati et al. [27] on nZVI coated with industrial minerals such as kaolinite (K-nZVI), bentonite (B-nZVI), and perlite (P-nZVI).

In Nosrati et al. [27], different methods of antimony removal from water and wastewater were reviewed

and the zero-valent iron nanoparticles coated on industrial mineral were selected as an effective and low-cost material for removing antimony from wastewater. For the purposes of their study, zero-valent iron nanoparticles of 40–100 nm in size were synthesized by dropwise addition of the sodium borohydride solution to an iron(III) aqueous solution at ambient temperature and mixed with nitrogen gas. To avoid particle agglomeration and to enhance the product's environmental safe application, the nanoparticles were coated on bentonite and characterized by SEM/EDAX and BET. The experiments were carried out by intense mixing of the adsorbent with 10 ml of real/synthetic wastewater samples in 20-ml bottles. The effects of pH, contact time, temperature, and adsorbent dosage on antimony removal efficiency were investigated under intense mixing using a magnetic mixer. Finally, the effluents were filtered upon completion of the experiments and used for atomic absorption analysis.

Zero-valent iron powder is a strong reducing agent. Nano-zero-valent iron (nZVI) has the capability to degrade organic materials and to adsorb inorganic contaminants, and nZVI indicated a great potential for environmental remediation of contaminants in soils, sediments, and groundwater [9].

Tables 1 and 2 indicate the data at a constant temperature of 25˚C and an initial concentration of antimony at 31.82 mg/l. The zero-valent iron nanoparticles had diameters of 40–100 nm and specific surface of 43.34 square meters per gram. Also, when antimony adsorbed on the absorbents, the pH values were considered 1–2 and the absorbent values were 7.5–12.5 because the optimal values and the tests were conducted in these intervals [24].

3. Results and discussion

3.1. Simulating antimony absorption coated on K-nZVI

3.1.1. The effect of pH on antimony absorption

To simulate antimony absorption, the absorbency value was considered 7.5 g/l. Fig. 1 indicates the simulated and experimental values of antimony absorption at different pHs in the presence of K-nZVI in the surface complex formation model 2-pK DLM. By increasing the pH from 1 to 2, antimony absorption increased by 60–92.3%. Also, the results of 2-pK DLM modeling described that the simulation value of antimony absorption is at the highest value at pH 2, i.e. 92.3%, and the maximum absorption happened based on the Nosrati [24] experiment at pH 2, i.e. 93.06%, [24]. The coefficient of determination between the simulated and experimental data was $R^2 = 0.92$, the index of agreement (*IA*) and *P* were 0.97. Rakshit et al. studied the absorption of antimony on kaolinite and obtained a maximum absorption at pH 3 with a value of 95% [10]. Sarkar et al. [31] studied the absorption of mercury on client and obtained a maximum absorption at pH 4.4 [31]. In the conducted stimulation, the optimum pH was 2 and the highest absorption occurred in an acidic state.

3.1.2. The effect of K-nZVI concentration on antimony absorption

Since adsorption is primarily a surface phenomenon, the amount of surface area available for absorption and thus the adsorbent mass can significantly affect the adequacy and performance of adsorption [20]. Therefore, we simulated the effect of K-nZVI concentrations on antimony absorption at pH 2. Fig. 2 presents the simulated and experimental values of antimony absorption at different concentrations of K-nZVI in the surface complex formation model 2-pK DLM. By increasing the concentration of zero-valent iron nanoparticles from 7.5 to 12.5 g/l, the antimony absorption rate increased by 92–95.5%. The absorption rate above 90% may be due to the high effect of K-nZVI on absorption. The reason is the increased surface area of nZVI and the expansion of more interchangeable surfaces available for reaction with antimony ions in increased concentrations. The simulation value of antimony absorption was at its highest value at an adsorbent concentration of 7.5 g/l. The

Table 1
Experimental data at pH values of 1–2 [24,27]

pH	Antimony absorption percentage on K-nZVI	Antimony absorption percentage on B-nZV	Antimony absorption percentage on P-nZVI
1	65.77	72.23	66.04
1.25	73.74	85.98	82.84
1.5	80.8	94.29	93.54
1.75	87.68	95.85	98.32
2	93.06	94.8	96.79

Table 2
Experimental data on adsorbent concentration of 7.5–12.5 (g/L) [24,27]

Adsorbent concentration (g/l)	Antimony absorption percentage on K-nZVI	Antimony absorption percentage on B-nZVI	Antimony absorption percentage on P-nZVI
7.5	93.06	82.5	91.5
8.5	93.4	88.1	94.57
9.5	93.8	92.36	96.9
10.5	94.5	95.28	97.9
11.5	95.31	96	96.97
12.5	95.5	96.85	95.44

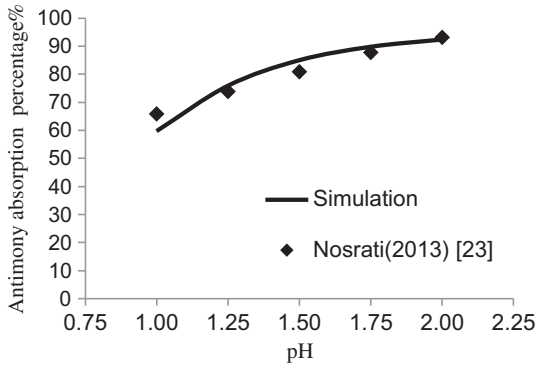

Fig. 1. The effect of pH on the absorption of antimony in the presence of a surface complex formation model 2-pK DLM (R^2 = 0.92 and P = 4.08).

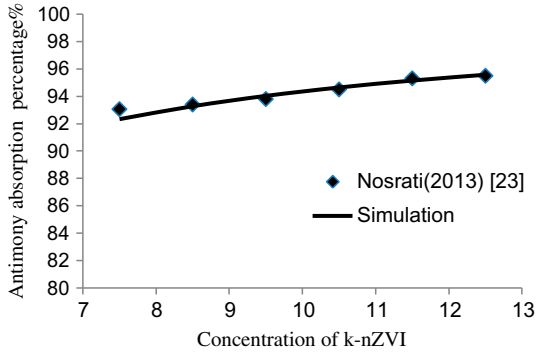

Fig. 2. The effect of concentration of k-nZVI on the absorption of antimony on surface complex formation model 2-pK DLM (R^2 = 0.97 and P = 0.37).

coefficient of determination between the simulated and experimental data was R^2 = 0.97. The index of agreement was IA = 0.99 and P was 0.37.

According to the Nosrati [24] experiment, the highest antimony absorption on K-nZVI was 93.06% at pH 2 at an adsorbent concentration of 7.5 g/l and an antimony absorption capacity of 3.94 mg/g. The results of the simulation presented the highest absorption of 92.33% at pH 2 at an adsorbent concentration of 7.5 g/l and an absorption capacity of 3.92 mg/g.

3.2. Simulating antimony absorption coated on B-nZVI

3.2.1. The effect of pH on antimony absorption

To simulate antimony absorption, the absorbency value was considered 10 g/l. Fig. 3 indicates the simulated and experimental values of antimony absorption at different pHs in the presence of B-nZVI in the surface complex formation model 2-pK DLM. By increasing the pH from 1 to 2, the antimony absorption increased by 70–96%. Also, the results of 2-pK DLM modeling showed that the simulation value of antimony absorption is at the highest value at pH 2, i.e. 96%; however, the maximum absorption happened based on the Nosrati [24] experiment and Nosrati et al. [27] at pH 1.75, i.e. 95.85% [27]. The coefficient of determination between the simulated and experimental data was R^2 = 0.98 and the index of agreement (IA) was 0.99. Vithanage et al. analyzed the antimony absorption on iron oxide coated in clay concluded that the highest absorbed Sb(V) is at pH 4–6 [19], and that in our study, occurred at pH 2.

3.2.2. The effect of B-nZVI concentrations on antimony absorption

We simulated the effect of B-nZVI concentrations on antimony absorption at pH 1.75. Fig. 4 presents the

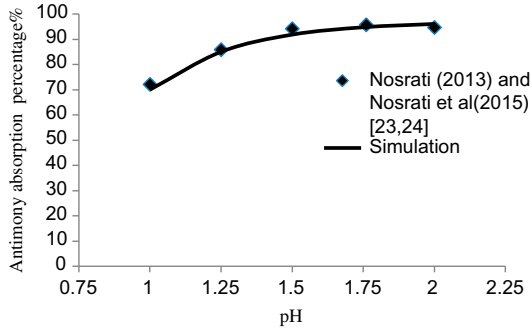

Fig. 3. The effect of pH on the absorption of antimony in the presence of a surface complex formation model 2-pK DLM (R^2 = 0.98 and P = 1.82).

simulated and experimental values of antimony absorption at different concentrations of B-nZVI in the surface complex formation model 2-pK DLM. By increasing the concentration of zero-valent iron nanoparticles from 7.5 to 12.5 g/l, the antimony absorption rate increased by 92–95%. The simulation value of antimony absorption was at the highest value at the adsorbent concentration of 12.5 g/l. The coefficient of determination between the simulated and experimental data was $R^2 = 0.94$. The index of agreement (*IA*) was 0.93 and P was 2.08.

According to the Nosrati [24] experiment and Nosrati et al. [27], the highest antimony absorption on B-nZVI was 96.85% at pH 1.75 at an adsorbent concentration of 12.5 g/l and the antimony absorption capacity of 2.54 mg/g. The results of the simulation indicated the highest absorption of 96.45% occurred at pH 2 at the adsorbent concentration of 12.5 g/l and an absorption capacity of 2.46 mg/g.

3.3. Simulating antimony absorption coated on P-nZVI

3.3.1. The effect of pH on antimony absorption

To simulate antimony absorption, the absorbency value was considered 10 g/l. Fig. 5 presents the simulated and experimental values of antimony absorption at different pHs in the presence of P-nZVI in the surface complex formation model 2-pK DLM. By increasing the pH from 1 to 2, the antimony absorption increased by 74–97.2%. Also, the results of 2-pK DLM modeling describe that the simulation value of antimony absorption was at the highest value at pH 1.75, i.e. 97.2%. The maximum absorption happened based on the Nosrati [24] experiment at pH 1.75, i.e. 98% [27]. The coefficient of determination between the simulated and experimental data was $R^2 = 0.96$; *IA* was 0.95 and *P* was 4.38.

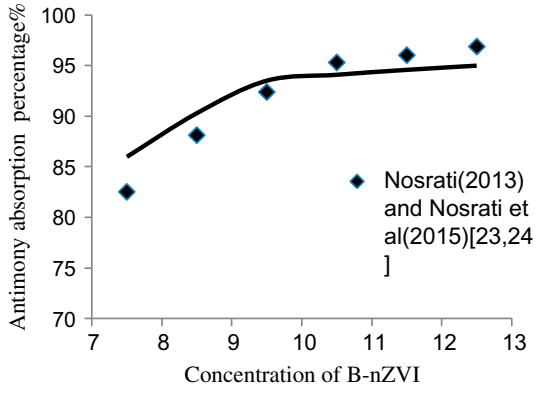

Fig. 4. The effect of concentration of B-nZVI on the absorption of antimony on surface complex formation model 2-pK DLM ($R^2 = 0.94$ and $P = 2.08$).

3.3.2. The effect of P-nZVI concentrations on antimony absorption

We simulated the effect of P-nZVI concentrations of antimony absorption at pH 1.75. Fig. 6 illustrates the simulated and experimental values of antimony absorption at different concentrations of P-nZVI in the surface complex formation model 2-pK DLM. By increasing concentrations of zero-valent iron nanoparticles from 7.5 to 12.5 g/l, the antimony absorption rate increased by 94–97%. The simulation value of antimony absorption was at the highest value at the adsorbent concentration of 10.5 g/l and then antimony absorption decreased. The coefficient of determination between the simulated and experimental data was $R^2 = 0.92$. The index of agreement (*IA*) was 0.90 and *P* was 1.52. Dorjee et al. analyzed antimony absorption on zero-valent iron nanoparticles and concluded that nZVI at concentrations greater than 0.1 mg quickly attracted more than 90%, which may be due to a high effect of nZVI in absorption [9]. In the present simulation, the effect of absorbent was high and has absorbed antimony content above 90%.

According to the Nosrati [24] experiment, the highest antimony absorption on P-nZVI was 97.90% at pH 1.75 at an adsorbent concentration of 10.5 g/l and an antimony absorption capacity of 3.16 mg/g. The results of the simulation indicated the highest absorption of 97.2% at pH 1.75 at the adsorbent concentration of 10.5 g/l and an absorption capacity of 3.10 mg/g.

Antimony is more serious in Azerbaijan province, Iran, owing to the existence of a large number of antimony mines. However, despite the evident potential Sb(V), its adsorption simulation from Zarshouran Gold Mineral Processing Plant (Iran) Wastewater by nano-zero valent iron coated on industrial mineral has not been reported to date. Saeidnia [32] indicated that using Dorjee et al.'s [9] and Rakshit's [10] experimental results to simulate Sb(V) adsorption on zero-valent iron nanoparticles coated on bentonite at different

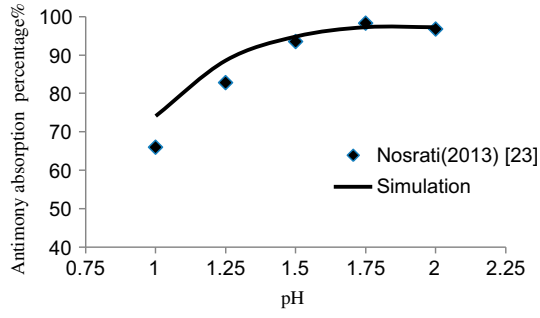

Fig. 5. The effect of pH on the absorption of antimony in the presence of a surface complex formation model 2-pK DLM ($R^2 = 0.96$ and $P = 4.38$).

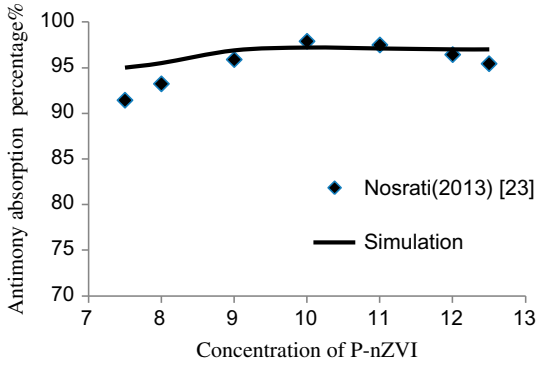

Fig. 6. The effect of concentration of P-nZVI on the absorption of antimony on the surface complex formation model 2-pK DLM (R^2 = 0.92 and P = 1.52).

pHs using VISUAL MINTEQ 3.1 software had a good agreement with the simulation using Nosrati et al.'s [27] results [32]. The coefficient of determination (R^2) between the simulated and experimental data using Dorjee et al. [9] and Rakshit [10] results on Sb(V) adsorption at different pHs was R^2 = 0.96 and IA was 0.98. These results have a good agreement with simulation of our study.

4. Conclusions

The results of simulation of antimony absorption on nZVI coated with industrial minerals (kaolinite, bentonite, and perlite) from mineral effluent using the VISUAL MINTEQ 3.1 software are as follows:

(1) In analyzing the effect of nanoparticles of zero-valent iron concentrations and the pH value, the coefficient of determination between the experimental data and the simulation value was above 0.9 which indicates the acceptability of our simulation.
(2) The results of the simulation indicated that by increasing the pH from 1 to 2, the antimony absorption on K-nZVI increased and the highest absorption of K-nZVI was 92.33% at pH 2 at an adsorbent concentration of 7.5 g/l and an absorption capacity of 3.92 mg/g which were in line with laboratory experiments.
(3) The results of the simulation described the highest absorption on B-nZVI was 96.45% at pH 2 at the adsorbent concentration of 12.5 g/l and absorption capacity of 2.46 mg/g which are in line with laboratory experiments.
(4) The results of our simulation indicated the highest absorption of P-nZVI was 97.2% at pH 1.75 at an adsorbent concentration of 10.5 g/l and an absorption capacity of 3.1 mg/g which were in line with laboratory experiments.
(5) The maximum antimony absorption simulation from the mineral wastewater was 97.2% related to the P-nZVI composite and the highest absorption capacity with the value of 3.92 of adsorbent was related to the K-nZVI composite. The results were consistent with the experimental results.
(6) Based on the experimental results and the simulation of antimony absorption, we may state that the pH and zero-valent iron nanoparticles have high performance in antimony absorption.
(7) The simulation results using VISUAL MINTEQ 3.1 software and using the surface complex formation model 2-pK DLM are consistent with laboratory works.

Acknowledgment

We wish to acknowledge Mr Ernest Rammel for assistant in editing our manuscript.

References

[1] M. Esanlou, Reconstruction of Mine, Amirkabir University Press, Tehran, 2001.
[2] M. Tabrizi, Geological Survey Organization of Iran, Ministry of Industry and Mines, Department of Geology and Environmental, Environmental Impact Assessment Reports and the Concentration of Heavy Metals in a Number of Villages in West Bijar Springs, Summer, 2001, p. 19.
[3] P. Hantson, N. Gurnani, A. Sharma, G. Talukder, Cytogenetic observations after meglumine antimoniate therapy for visceral leishmaniasis, Pharmacotherapy, J. Human Pharmacol. Drug Ther. 16(5) (1996) 869–871.
[4] J.L. Wardell, Arsenic, antimony, and bismuth, in organometallic chemistry, R. Soc. Chem. 51976 (2005) 157–165.
[5] Z. Pawlak, S. Zack, L. Zablocki, Removal of hazardous metals from groundwater by reverse osmosis, Pol. J. Environ. Stud. 15(4) (2006) 579–583.
[6] E.A. Deliyanni, D.N. Bakoyannakis, A.I. Zouboulis, K.A. Matis, Sorption of As(V) ions by akaganéite-type nanocrystals, Chemosphere 50(1) (2003) 155–163.
[7] R. Djeribi, O. Hamdaoui, Sorption of copper(II) from aqueous solutions by cedar sawdust and crushed brick, Desalination 225 (2008) 95–112.
[8] G. Aragay, A. Merkoçi, Nanomaterials application in electrochemical detection of heavy metals, Electrochim. Acta 84 (2012) 49–61.
[9] P. Dorjee, D. Amarasiriwardena, B. Xing, Antimony adsorption by zero-valent iron nanoparticles (nZVI): Ion chromatography–inductively coupled plasma mass spectrometry (IC–ICP-MS) study, Microchem. J. 116 (2014) 15–23.

[10] S. Rakshit, D. Sarkar, R. Datta, Surface complexation of antimony on kaolinite, Chemosphere 119 (2014) 349–354.
[11] Ç. Üzüm, T. Shahwan, A.E. Eroğlu, K.R. Hallam, T.B. Scott, I. Lieberwirth, Synthesis and characterization of kaolinite-supported zero-valent iron nanoparticles and their application for the removal of aqueous Cu^{2+} and Co^{2+} ions, Appl. Clay Sci. 43(2) (2009) 172–181.
[12] J. Ilavsky, Removal of antimony from water by sorbtion materials, Slovak J. Civ. Eng. 2 (2008) 1–6.
[13] A. Anjum, M. Datta, Adsorptive removal of antimony (III) using modified montmorillonite: A study on sorption kinetics, J. Anal. Sci., Methods Instrum. 2 (2012) 167–175.
[14] Y. Leng, W. Guo, S. Su, C. Yi, L. Xing, Removal of antimony(III) from aqueous solution by graphene as an adsorbent, Chem. Eng. J. 211–212(5) (2012) 406–411.
[15] M.A. Salam, R.M. Mohamed, Removal of antimony (III) by multi-walled carbon nanotubes from model solution and environmental samples, Chem. Eng. Res. Des. 91(7) (2013) 1352–1360.
[16] A. Sari, G. Sahinoglu, M. Tuzen, Antimony(III) adsorption from aqueous solution using raw perlite and Mn-modified perlite: Equilibrium, thermodynamic, and kinetic studies, Ind. Eng. Chem. Res. 51 (19) (2012) 6877–6886.
[17] J. Xi, M. He, C. Lin, Adsorption of antimony(V) on kaolinite as a function of pH, ionic strength and humic acid, Environ. Earth Sci. 60(4) (2010) 715–722.
[18] M. Vithanage, A. Rajapaksha, Surface complexation modeling and spectroscopic evidence of antimony adsorption on iron-oxide-rich red earth soils, J. Colloid Interface Sci. 406 (2013) 217–224.
[19] B. Safavi, Mathematical Study for Determination of Effective Parameters for Removal of Cyanide from Artificial Wastewater using Nanoparticle Titanium Dioxide, M.S Thesis, University of Kharazmi, Tehran, 2014 (in Farsi).
[20] A Geoscience Hydro geologic, Inc. Herndon, Virginia MINTEQA2/PRODEFA2, A Geochemical Assessment Model for Environmental Systems: User Manual Supplement for Version 4.0, Prepared for the U.S. Environmental Protection Agency, National Exposure Research Laboratory, Ecosystems Research Division, Athens, Georgia, 1998.
[21] M. Davoodi, The Interaction of Iron and Phosphate Adsorption on Geonite, PhD Thesis, Tarbiat Modares University, Tehran, 2010.
[22] W. Stumm, C.P. Huang, S.R. Jenkins, Specific chemical interaction affecting the stability of dispersed systems, Croat. Chem. Acta 42 (1970) 223–245.
[23] D.A. Dzomback, F.M. Morel, Surface Complexation Modeling: Hydrous Ferric Oxide, Jon Wiley and Sons, New York, NY, 1990.
[24] N. Nosrati, Antimony adsorption from Zarshouran gold mineral processing plant wastewater by nano zero valent iron coated on industrial minerals, M.S Thesis, Department of Mining Engineering, Tarbiat Modares University, Tehran, 2013.
[25] G. Gouy, Sur la constitution de la charge electrique a la New York. surface d'un electrolyte, Compt. Rend. 149 (1909) 654–657.
[26] D.L. Chapman, A contribution to the theory of electrocapillarity, Phil. Mag. 25 (1913) 475–481.
[27] N. Nosrati, A. Khodadadi Darban, M. Abdollahi, Antimony adsorption from Zarshouran Gold Mineral processing plant wastewater by nano zero valent iron coated on Bentonite, J. Water Wastewater 26(1) (2015) 46–56 (in Farsi).
[28] J.J. Heckman, Sample selection bias as a specification error, Econometrica 47(1) (1979) 153–162.
[29] P. Krause, D.P. Boyle, F. Bäse, Comparison of different efficiency criteria for hydrological model assessment, Adv. Geosci. 5 (2005) 89–97.
[30] C.J. Willmott, S.M. Robeson, K. Matsuura, A refined index of model performance, Int. J. Climatol. 32(13) (2012) 2088–2094.
[31] D. Sarkar, M.E. Essington, K.C. Misra, Adsorption of mercury(II) by variable charge surfaces of quartz and gibbsite, Soil Sci. Soc. Am. J. 63 (1999) 1626–1636.
[32] S. Saeidnia, Simulation Study on Effective Parameters on Existing Antimony Adsorption of Mineral Wastewater using Zero-Valent Iron, Master Thesis, Kharazmi University, Iran, 2014.